# We are IntechOpen,
# the world's leading publisher of
# Open Access books
# Built by scientists, for scientists

## 6,100
Open access books available

## 149,000
International authors and editors

## 185M
Downloads

Our authors are among the

## 154
Countries delivered to

## TOP 1%
most cited scientists

## 12.2%
Contributors from top 500 universities

CLARIVATE ANALYTICS
**BOOK CITATION INDEX**
INDEXED

**WEB OF SCIENCE**™

Selection of our books indexed in the Book Citation Index
in Web of Science™ Core Collection (BKCI)

# Interested in publishing with us?
# Contact book.department@intechopen.com

**Chapter**

# Surface Analysis of Graphene and Graphite

*Wenjing Xie and Chi-Ming Chan*

## Abstract

Graphene and graphite are two widely studied carbon materials. Due to their particular properties and structure, graphene and graphite have been used in a variety of fields such as electronic devices and sensors. The surface properties of graphene and graphite as well as their derivatives are strongly connected to the performances of devices and sensors. Thus, it is necessary to choose appropriate surface analysis techniques for characterization, which are not only useful in the understanding of the surface composition and structure but also in the design and development of these types of materials. X-ray photoelectron spectroscopy (XPS) and time-of-flight secondary ion mass spectrometry (ToF-SIMS) have been two of the key surface analysis techniques that are widely used to characterize these surfaces. In this chapter, an overview of the applications of XPS and ToF-SIMS in the study of the surfaces of graphene and graphite is present. We hope that the information provided will simulate more exciting and inspiring research on graphene and graphite and promote practical applications of these carbon materials in the future.

**Keywords:** graphene, graphite, surface, XPS, ToF-SIMS

## 1. Introduction

Carbon materials have been widely used to promote technological advances in various applications such as energy storage, catalysis, and sensors. These materials which are mainly composed of carbon atoms exhibit diverse structures and properties depending on the valence bond hybridization of carbon. As a new member of carbon materials, graphene exhibits extraordinary physical and chemical properties. Graphene is a zero-bandgap semiconductor and exhibits room temperature electron mobility, which is much higher than those of silicon or other semiconductors and weakly affected by temperature and doping effect [1]. These properties impart the rapid development of graphene-based transistors or integrated circuits which are considered as a promising alternative to silicon electronics [1, 2]. The first graphene-based circuit was developed by Lin *et al.* in 2011 [3]. The graphene integrated circuit operates as a broadband radio-frequency mixer at frequencies up to 10 gigahertz and exhibits outstanding thermal stability. Graphene is highly optically transparent and absorbs only 2.3% of the incident white light [4]. Graphene also displays the highest thermal conductivity compared to other carbon materials [5]. Thus, graphene has applications for transparent touchscreens, organic light-emitting diodes as well

as solar cells. Large-area, continuous, transparent, and highly conductive graphene, which can be produced by chemical vapor deposition (CVD) method, is used as an anode in photovoltaic devices with a power conversion efficiency of up to 1.71% [6]. The large specific surface area, flexibility, and high electrical conductivity of graphene make it an ideal material for sensors [7]. In particular, the graphene sensor for COVID-19 detection can detect viruses faster and more accurate [7]. For example, a graphene-based field-effect transistor biosensing device was created to detect spike protein on COVID-19 with a limit of detection of 1 fg mL$^{-1}$ [8]. Graphene has a unique two-dimensional (2D) single-sheet structure and is considered a building block of other carbon allotropes. It can be wrapped up into zero-dimensional (0D) fullerene, rolled into one-dimensional (1D) carbon nanotube, or stacked into three-dimensional (3D) graphite [1]. In the graphite structure, each carbon atom is sp$^2$ hybridized. The highly oriented pyrolytic graphite (HOPG) is a highly-ordered and high-purity form of synthetic graphite. A new HOPG surface can be generated *via* simple tape cleavage. It is an ideal model to be used as a calibration standard for microscopic imaging [9, 10], and a substrate for chemical reactions [11] and surface modifications by laser irradiation and ion beam bombardment [12].

It is well known that the surface physical and chemical properties of materials are quite different from those of their bulks. Many critical physical and chemical reactions occur on surfaces of materials, such as oxidation, contamination, corrosion, and adsorption. As surface properties are governed by the atomic structure and composition of the outermost layer of the surface of a material, it is necessary to use appropriate surface analysis techniques for its characterization. X-ray photoelectron spectroscopy (XPS) is a widely used surface analysis technique with a sampling depth of 2–10 nm because of its simplicity in use and straightforward in data interpretation [13, 14]. It provides nondestructive quantitative information with an accuracy of up to 0.1 at% on the elemental composition and the chemical state of the elements present on the surface of a material. When high-sensitivity elemental analysis and spatial distribution information of chemical species on a surface are needed, an extremely surface-sensitive technique with a sampling depth of approximately 1 nm, the spatial resolution of about 0.1 μm, and low detection limit up to ppm called time-of-flight secondary ion mass spectrometry (ToF-SIMS) is applied [13, 14]. The secondary fragments generated from the surface of a material are related to its surface chemical structure, such as defects and the functional groups at its edges. However, quantitative information can hardly be deduced from the ion intensities and data interpretation is more complicated. Therefore, a combination of XPS and ToF-SIMS can provide complementary details about the chemical information of the surface of a material.

The objective of this chapter is to present an overview of the applications of XPS and ToF-SIMS in the surface characterization of graphene and graphite, including their preparation processes, impurities, surface defects as well as their surface reactions. We hope this chapter will drive a deeper understanding of graphene and graphite surfaces for faster development and wider applications of these types of materials.

## 2. Synthesis of graphene

The high spatial resolution imaging and chemical specificity of ToF-SIMS make it a suitable tool to investigate the uniformity of graphene and determine the number of graphene layers. The high spatial resolution map using the C$_2^-$ ion as a marker for
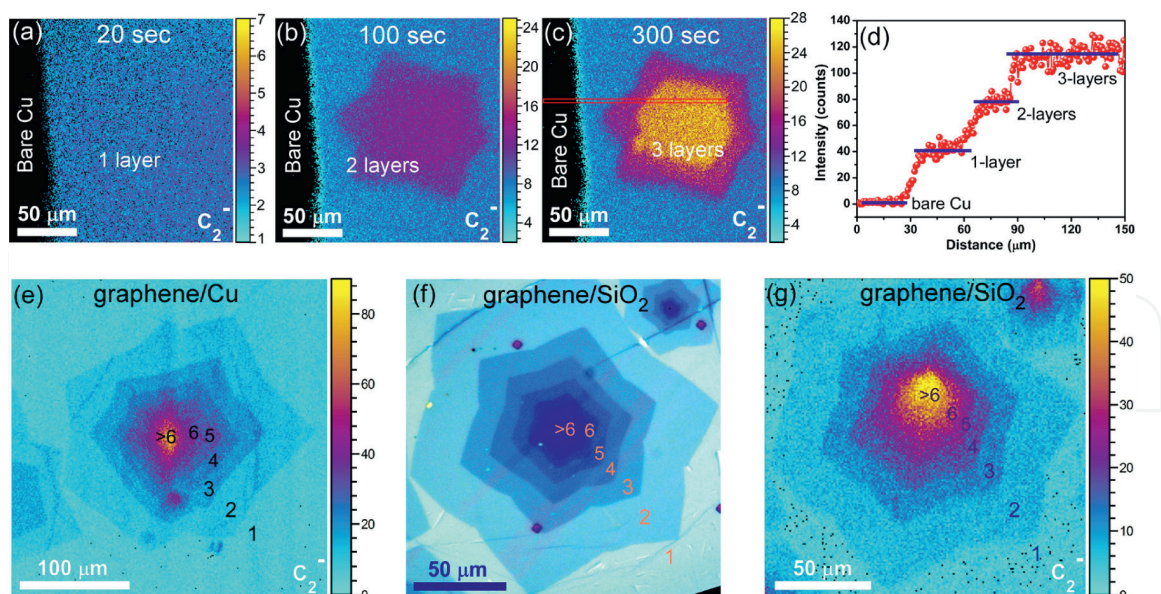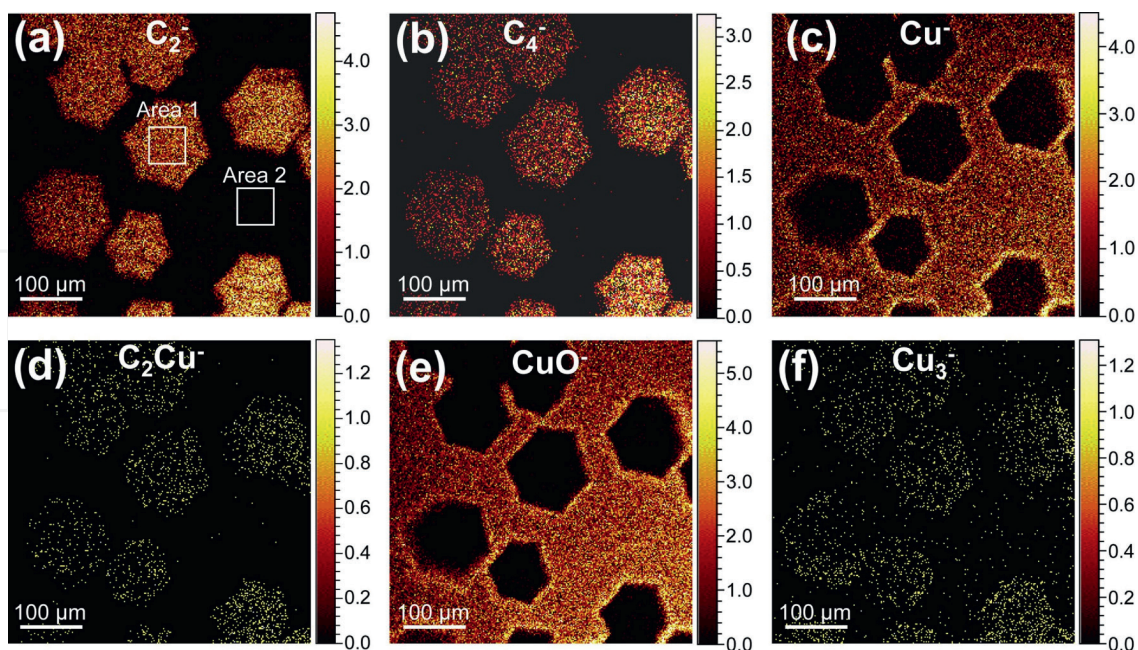
**Figure 1.**
*The $C_2^-$ ion map was reconstructed by accumulating the signals for (a) 20 s, (b) 100 s, and (c) 300 s of $Cs^+$ sputtering, respectively. (d) A plot of the $C_2^-$ ion intensity integrated from the area line scan is shown in (c). (e) ToF-SIMS $C_2^-$ ion image of graphene on a Cu substrate. (f) Optical image and (g) corresponding ToF-SIMS $C_2^-$ ion image of graphene on a $SiO_2$/Si substrate [15].*

the hexagonal graphene domains provides information about the uniformity of its domains [15]. In addition, ToF-SIMS analysis of multilayer graphene was achieved by cycles of high lateral resolution imaging followed by slow $Cs^+$ ion sputtering to remove the graphene materials [15]. As shown in **Figure 1**, with 20 s of sputtering time, a uniform graphene layer can be observed, while it takes approximately 100 s of sputtering for the removal of the first layer of graphene. Prolonging the sputtering for a longer time exposes all the buried adlayers underneath the top layer, and thus a total of three layers of graphene can be observed after accumulating $C_2^-$ signals for 300 s of sputtering. The intensity of the $C_2^-$ ion shows a stepwise increase with the number of graphene layers. Particularly, the $C_2^-$ ion intensity at each step shows a linearly proportional increase to the number of graphene layers, and up to six layers of graphene can be distinguished. These results are validated with analogous optical images showing six layers of graphene. The ToF-SIMS chemical image shows its capability of identifying the layer number of graphene on both $Si/SiO_2$ and Cu substrates.

CVD has been commonly used to grow large-area graphene sheets on various metal substrates [16]. Cu foil is often chosen as a substrate and also a catalyst for monolayer graphene growth [17]. The weak interaction between the graphene and Cu foil allows the graphene films to expand over the grain boundaries with minimal structural disruption, resulting in electron transfer from the Cu foil to the graphene [16, 18]. ToF-SIMS is a suitable technique to determine the chemical structures created from this interaction. It was found that peaks related to the interaction between the graphene and Cu foil substrate, such as $C_2Cu^-$ and $C_4Cu^-$ ions, are present in the ToF-SIMS negative ion spectrum obtained at 450°C [19]. The ToF-SIMS images further verify that the $C_2Cu^-$ ion shows a distribution pattern similar to that of the $C_2^-$ ion, which is a characteristic ion for graphene (**Figure 2**). Two areas (60 μm × 60 μm) from the ToF-SIMS image of the $C_2^-$ ion corresponded to areas with high graphene and Cu concentrations were then picked for analysis. Both the graphene-related peaks, i.e., the $C_x^-$ and $C_xH^-$ (where x=1, 2, 3...) ion series, and

**Figure 2.**
*ToF-SIMS images of different ions of graphene on a Cu foil substrate: (a) $C_2^-$, (b) $C_4^-$, (c) $Cu^-$, (d) $C_2Cu^-$, (e) $CuO^-$ and (f) $Cu_3^-$ ions [19].*

peaks related to the interaction between the graphene and Cu foil substrate ($C_xCu^-$ ion series) have higher intensities in the areas with a higher graphene concentration, confirming the existence of the graphene-Cu interaction at the interface of the graphene and Cu foil substrate.

Moreover, the oxidation protection of graphene for the Cu foil substrate was found when comparing the ToF-SIMS negative ion spectra obtained from the areas with and without graphene coverage [19]. The intensities of the peaks related to the oxidation of the Cu foil substrate, such as the $CuO^-$ and $Cu_2O^-$ ions, are significantly higher in the spectrum obtained from the area without graphene coverage. On the contrary, the ion intensity ratios of Cu cluster ions to the $Cu^-$ ion, such as the $Cu_3^-/Cu^-$ and $Cu_4^-/Cu^-$, are higher in the area with a higher graphene concentration. The $Cu_3^-$ ion shows a distribution pattern similar to that of the $C_2^-$ ion but complementary to that of the $CuO^-$ ion (**Figure 2**). As the metal cluster ions are usually generated during the sputtering process by direct ejection from a metal surface, it can be anticipated that more Cu cluster ions are formed from pure metal than from its oxides. Therefore, the higher ion intensity ratios of Cu cluster ions to the $Cu^-$ ion in the areas with a high graphene concentration also confirm that less oxidation occurred in the graphene-covered Cu foil substrate than in the uncovered areas. The above results confirm that the growth of graphene on a Cu foil substrate can prevent oxidation of the Cu foil substrate during storage and annealing processes. The graphene on the Cu foil substrate can inhibit the diffusion of small molecules, such as $O_2$ and $H_2O$, into the interface between the graphene and Cu foil substrate, thus preventing the oxidation of the copper.

## 3. Impurities in graphene and graphite

To better measure the optical and electronic properties of graphene, the graphene grown on a Cu foil needs to be transferred onto another target substrate, such as Si wafer or glass. During the transfer processes, a polymer such as poly(methyl methacrylate)

(PMMA) is commonly used as a membrane support to prevent folding or tearing of graphene [20, 21]. Studies have shown that there is still some residual PMMA remaining on the surface of graphene after cleaning by chemical or thermal treatment [22, 23]. When exposed in the air or during XPS and ToF-SIMS measurements at room temperature, the adsorption of hydrocarbon and oxygen contaminants on the graphene and graphite surfaces is very likely. Xie *et al.* developed a process to produce a very clean graphene surface through annealing a graphene sample at 500°C in an ultra-high vacuum chamber without creating any additional defects [24]. XPS was used to estimate the residual PMMA and hydrocarbon contaminants on the graphene surface before and after annealing at different temperatures based on the curve-fitting results. The XPS results indicate that a clean surface was produced after annealing the sample at 500°C for 45 min. A similar experiment was repeated, and the sample was analyzed by ToF-SIMS. After selecting representative ions of PMMA and hydrocarbons from ToF-SIMS spectra, such as $C_2H_3O_2^+$ and $CH_3O^-$ for PMMA and $C_4H_5^+$ for hydrocarbons, and calculating their normalized intensities under different annealing conditions, the results confirmed that the residual PMMA can be removed from the surface of graphene at 400°C, while hydrocarbon contaminants require a higher temperature of 500°C to remove.

Furthermore, by using deuterium isotope-labeled PMMA and ToF-SIMS, the residual PMMA on a graphene surface was identified, located, and quantified. **Figure 3** shows ToF-SIMS depth profiles and high lateral resolution maps of $C_3^-$ ion representing graphene and $^2H^-$ ion representing deuterated-PMMA [25]. As shown in the depth profiles, the $^2H^-$ ion is concentrated on the top surface and its intensity drops when penetrating into the graphene structure. The $C_3^-$ ion increases gradually and reaches a maximum at the depth of about 0.2 nm ($^2H^-$ ion with relatively low intensity), and then gradually decreases when going into the $SiO_2$ substrate layer. The mapping results, as shown in **Figure 3b** and **c**, indicate that the $^2H^-$ ion appears mainly in the same areas where the $C_3^-$ ion is present, confirming that the residual PMMA is present on the graphene surface.

In addition, metallic impurities introduced during the transfer process can lead to contamination of fabrication devices. The out-diffusing of these impurities toward the substrate during the device processing can result in degradation of the device parts located beneath graphene. ToF-SIMS was used to detect Cu and Fe residuals originating from the transfer process of graphene [26]. The ToF-SIMS images of transferred graphene showed the presence of Cu and Fe residuals on the areas covered with graphene. A comparison of ToF-SIMS mass spectra between the $SiO_2$/Si
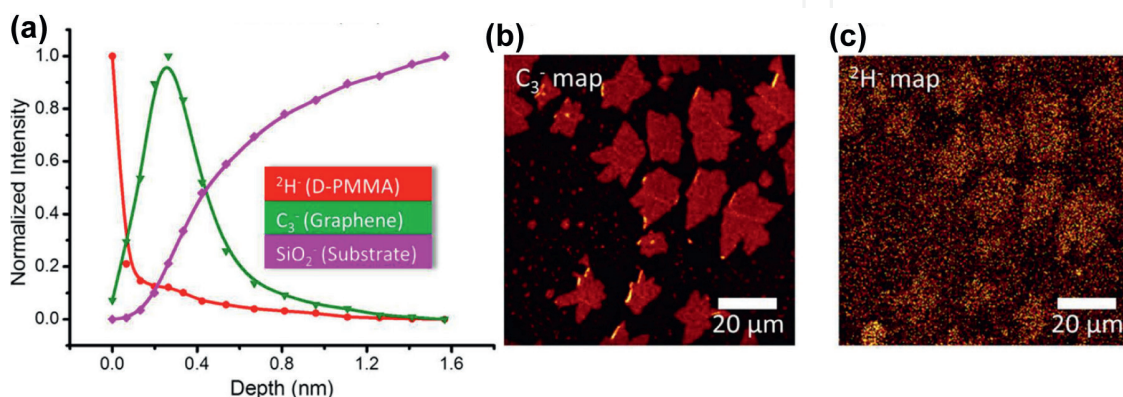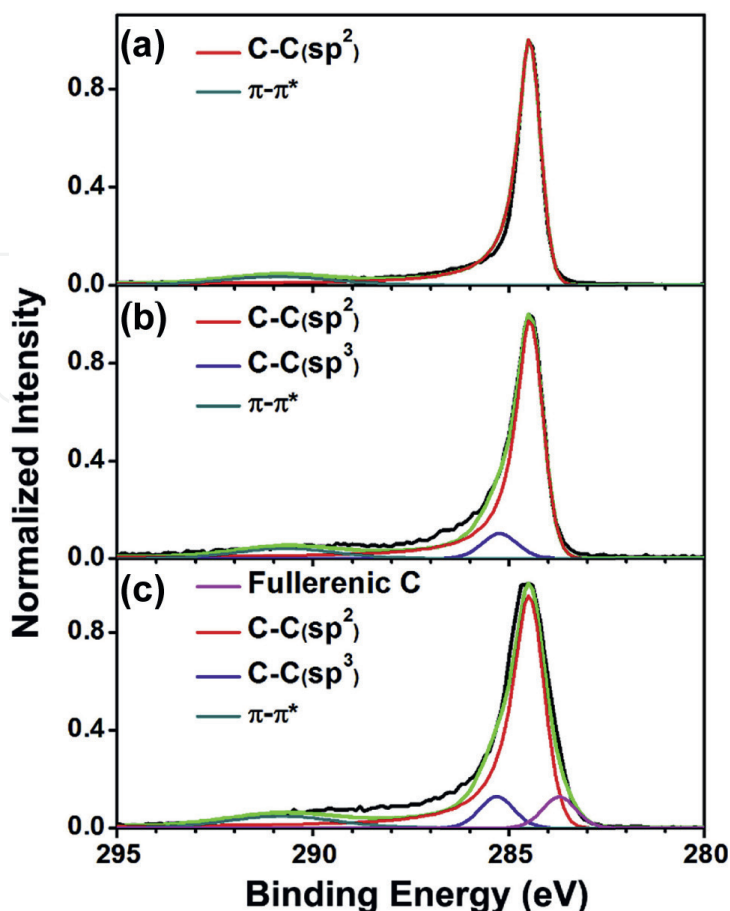


**Figure 3.**
*(a) ToF-SIMS depth profiles of $^2H^-$, $C_3^-$ and $SiO_2^-$ ions. ToF-SIMS images of (b) $C_3^-$ and (c) $^2H^-$ ions [25].*

substrates with and without graphene confirmed that the presence of residual metals is related to the graphene transfer process. Combined with total reflection X-ray fluorescence, the residual metal (Cu and Fe) concentrations were calculated to be approximately $10^{13}$–$10^{14}$ atoms cm$^{-2}$ regardless of the transfer method.

## 4. Defects in graphene and graphite

Studies have shown that defects can arise during the preparation process of graphene. The defects in graphene exist in the form of sp$^3$ carbons with more or less than six carbon atoms in a ring [27]. Usually, one or two H atoms are attached to the sp$^3$ carbons. The presence of defects in graphene can change its electrical, mechanical and magnetic properties as well as surface chemical reactivities, thus having a significant impact on the performance of graphene-based devices. On the contrary, the surface of HOPG is almost defect-free with only delocalized sp$^2$ carbons and can be used as a standard model for the study of surface defects on graphene. XPS has been the preferred choice for determining the structures of graphene and graphite surfaces [28]. **Figure 4a** shows an XPS C1s spectrum of HOPG, revealing a narrow main carbon peak with the binding energy at 284.5 eV, accompanied by a broad and asymmetric tail toward higher binding energy [28]. The asymmetry is due to the low energy electron-hole pair excitation as the valence electrons respond to the presence of the core hole. Two empirical approaches have been used to curve fit this asymmetric line shape. The first approach uses an asymmetric Doniach-Sunjic function, which was originally developed for analyzing the asymmetric line shapes of XPS spectra of metals [29], while the other considers HOPG as a neutral alternant hydrocarbon and fits its C1s spectrum with five symmetric components [30]. Xie *et al.* obtained clean HOPG and graphene surfaces by annealing the samples at 500°C in an ultra-high vacuum chamber [28]. A combination of Doniach-Sunjic and Gaussian-Lorentzian functions was used to curve fit the asymmetric C1s spectrum of HOPG. An asymmetric parameter of 0.035 was determined after considering the left full-width-at-half maximum (FWHM$_{left}$) and the right FWHM (FWHM$_{right}$) of the C1s peak. The C1s spectrum of clean HOPG was fitted with two components including the sp$^2$ carbon peak and the $\pi$-$\pi^*$ shake-up peak (**Figure 4a**). However, for the curve-fitting of C1s spectrum of graphene, a sp$^3$ carbon peak representing the defects at the binding energy varying between 285.0 and 285.5 eV also appears (**Figure 4b**). To confirm the nature of the sp$^3$ peak, defects were introduced on the surface of HOPG. An effective way of inducing defects on the surface of HOPG is ion bombardment, in which the defect density can be controlled by varying the ion dose density. Defects created on a HOPG surface can broaden the FWHM of its XPS C1s spectrum and make the line shape on the high-binding-energy side of the peak more asymmetric due to the disorder of its delocalized sp$^2$ structure and the development of the sp$^3$ component. **Figure 4c** shows that the FWHM of the C1s peak becomes broader and the sp$^3$ carbon peak intensifies as more defects were created on the surface of HOPG. The C1s curve of the sputtered HOPG at the take-off angle of 20° (sampling depth about 2.6 nm) showed a higher sp$^3$ peak intensity compared with that at 90° (sampling depth about 7.5 nm). This result indicates that sp$^3$ defects which were created by sputtering a defect-free HOPG surface mainly concentrated on the top surface. The atomic ratio of sp$^3$ carbons to sp$^2$ carbons in the sputtered HOPG samples determined by XPS was used to estimate the amounts of sp$^3$ defects. For the HOPG sample, the ratio was close to zero. As the sputtering dose increased, the ratio gradually increased. Note
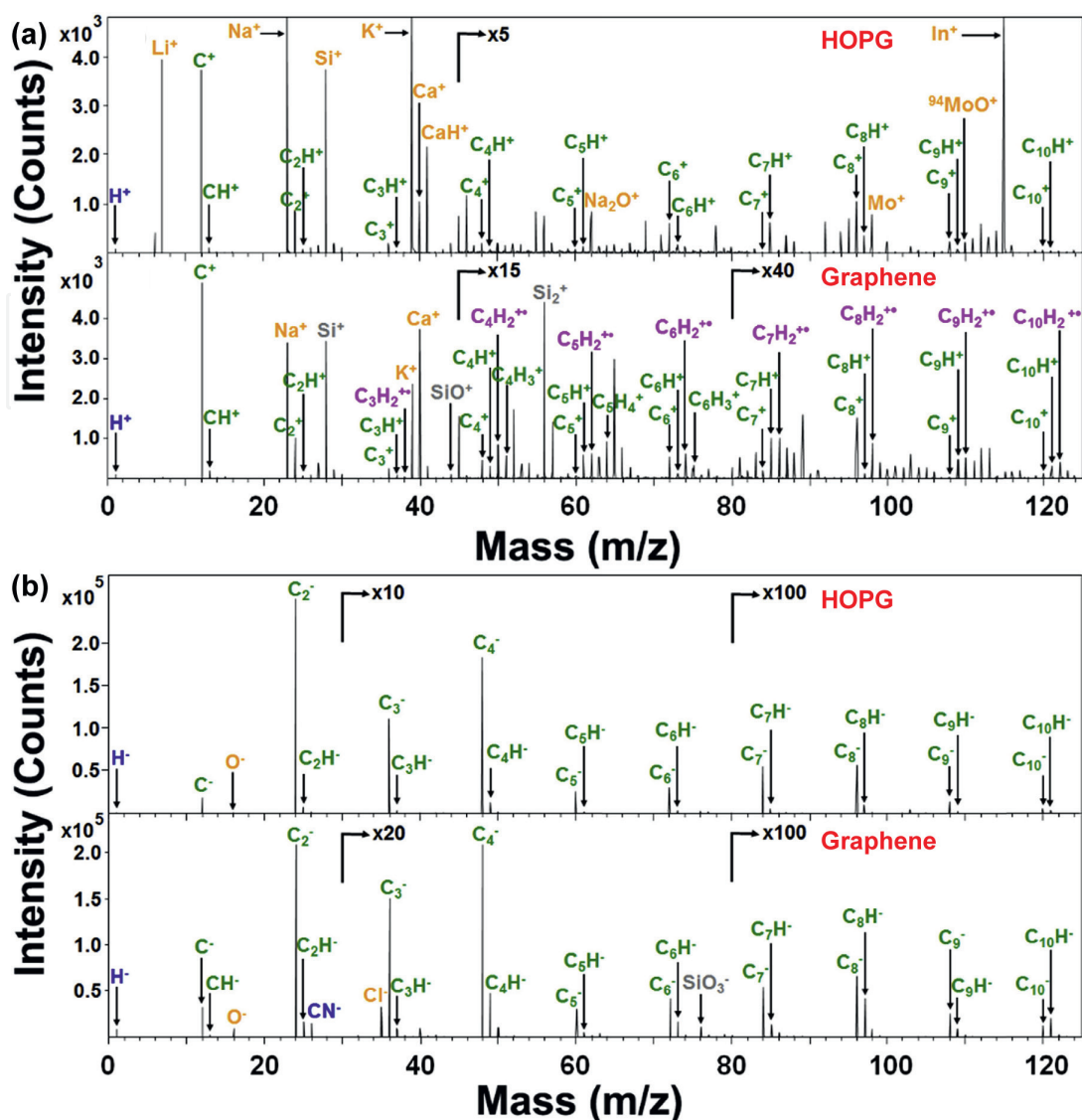
**Figure 4.**
*XPS C1s normalized spectra of (a) HOPG after 500°C annealing, (b) graphene on a SiO$_2$/Si wafer after washing with acetone and annealing at 500°C, and (c) HOPG after 500°C annealing followed by Ar$^+$ sputtering with a sputtering dose of 5.0 × 10$^{15}$ ions cm$^{-2}$. The black (—) and green (—) lines represent the experimental and curve-fitted spectra, respectively. All spectra were obtained at 500°C at a take-off angle of 20° [28].*

that sputtering creates defects but at the same time also removes the defects from the surface. As a result, the ratio eventually reached a constant value when the rate of defect generation equaled the rate of defect removal.

The defects in graphene can also be characterized using ToF-SIMS [28]. A comparison between the ToF-SIMS spectra of graphene and HOPG shows similar ions, including $C_x^+$, $C_xH^+$, $C_x^-$, and $C_xH^-$ (**Figure 5**). The typical fragment ions of graphene and HOPG can be categorized into several types. The $C_x^+$ and $C_x^-$ ion series are the type that mainly comes from the direct breaking up of the sp$^2$ areas of graphene and HOPG surfaces. The H-containing fragment ions ($C_xH^+$ and $C_xH^-$) form another type of typical fragment ions of graphene and HOPG. The $C_xH^+$ and $C_xH^-$ ions contain at least one hydrogen which would normally be absent from a defect-free graphene or HOPG surface. Their presence in the spectra suggests that they were created *via* direct ejection of the carbons at or near the defect areas of the graphene and HOPG surfaces. Since graphene has many more defects on its surface, the probability of formation of the $C_xH^+$ and $C_xH^-$ ions in graphene is higher, leading to their higher normalized intensities. Another major difference between the spectra of graphene and HOPG is that $C_xH_2^{+\cdot}$ ions are present in the positive ion spectrum of graphene but absent in the spectrum of clean HOPG. Therefore, it was suspected that the $C_xH_2^{+\cdot}$ ions might be generated at or near a defect in graphene. To further determine the origin of $C_xH_2^{+\cdot}$ ions, ion bombardment was carried out to create defects on a HOPG surface.
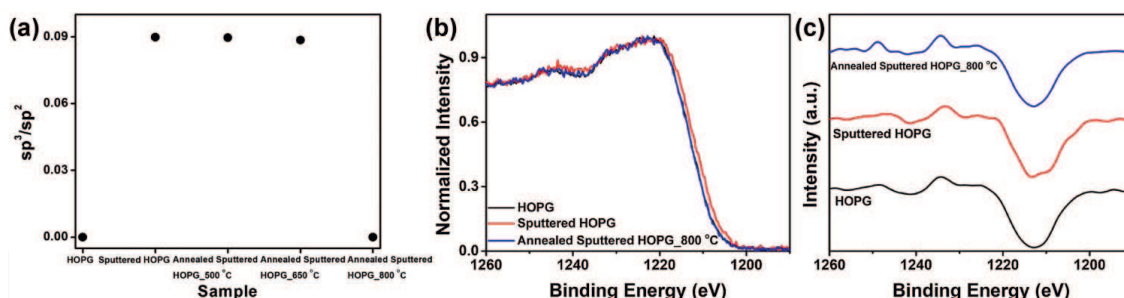
**Figure 5.**
*ToF-SIMS (a) positive and (b) negative ion spectra of HOPG after annealing at 500°C and graphene on a SiO₂/ Si wafer after washing with acetone and annealing at 500°C. All spectra were obtained at 500°C [28].*

A detailed examination of the positive ion spectra of ion-bombarded HOPG surfaces reveals the presence of the $C_xH_2^{+\cdot}$ ions, confirming that these ions originated from the defects created on the sputtered HOPG surfaces. Therefore, the $C_xH_2^{+\cdot}$ ions can be used as an indicator for the existence of defects in graphene and graphite surfaces.

Studies have shown that defects on graphite and graphene surfaces can be repaired under a carbon atmosphere, a noble gas atmosphere, or in a vacuum [31–33]. The repairs can improve their thermal and electrical conductivities and enhance their mechanical strength. Xie *et al.* revealed that the defects created on the surface of HOPG by ion bombarding can be repaired through high-temperature annealing [34]. Both XPS and ToF-SIMS were applied to monitor the creation and repair of defects in a HOPG surface. The ratio of $sp^3$ to $sp^2$ carbons was calculated from XPS results for the HOPG surface before and after sputtering as well as the sputtered HOPG surface after annealing under Ar at different temperatures. These results are shown in **Figure 6a**. This ratio is close to zero for the HOPG and increases to about 0.09 after a dose of $5.8\times10^{15}$ ions cm$^{-2}$ sputtering. After annealing at either 500 or 650°C, the ratio remains the same, but annealing at 800°C reduces the ratio to about zero. Therefore, defects on the surface of

**Figure 6.**
*(a) The ratio of sp³ to sp² carbons in the fresh HOPG sample, HOPG after Ar⁺ sputtering at a dose of 5.8 × 10¹⁵ ions cm⁻² and after annealing in Ar at different temperatures. (b) C KLL spectra of the fresh, sputtered, and annealed HOPGs and (c) their first derivatives obtained at 500°C [34].*

the sputtered HOPG can be repaired by annealing at 800°C in Ar. The ratio of the $sp^3$ to $sp^2$ carbons can be estimated using the distance between the most positive maximum and the most negative minimum of the first derivative of an XPS C KLL spectrum which is referred to as the D parameter [35, 36]. For HOPG, this value varies from 21.2 to 23.1 eV [35, 36]. As shown in **Figure 6b** and **c**, the calculated D parameters are 21.3 and 20.1 eV for the fresh and sputtered HOPG, respectively. The decrease of the D value implies an increase in the number of $sp^3$ carbons on the surface. After annealing at 800°C in Ar, the D value is 21.6 eV, which is similar to that of the fresh HOPG. The recovery of the D value for sputtered HOPG after annealing again implies the conversion of the $sp^3$ carbons which are present as defects on the sputtered sample to $sp^2$ carbons through annealing.

ToF-SIMS spectra were obtained from the surfaces of HOPG before and after Ar⁺ sputtering and the sputtered HOPG sample after annealing under flowing Ar at different temperatures [34]. The normalized intensity of the $C_xH_2^{+\cdot}$ ions was used as an indicator to reveal the concentration of the defects on the HOPG surfaces. It is obvious that the intensity of these ions was close to zero for the fresh HOPG because it is a defect-free surface. Interestingly, the intensity of these ions for the sputtered HOPG increased, indicating the creation of defects; while the intensity of these ions for sputtered HOPG after annealing at 800°C was close to zero except for the $CH_2^{+\cdot}$ and $C_2H_2^{+\cdot}$ ions, suggesting the healing of these defects created by sputtering.

## 5. Reactions on the surfaces of graphene and graphite

The performances of different reactions on graphene and graphite such as catalysis, oxidation and reduction, as well as functionalization, are dependent on their surface properties, which are the primary areas of interest. N-doped carbon materials are promising catalysts that exhibit high electrocatalytic activity for the oxygen reduction reaction with high durability [37]. By using HOPG as a model, several types of N-doped HOPG model catalysts were created to investigate the active sites in the oxygen reduction reaction [38]. These N-doped HOPG models included clean-HOPG, Ar⁺ ion sputtered HOPG and HOPG modified with different types of N such as pyridinic and graphitic N on the surface. The introduction of different types of N on the HOPG surface was verified by a least-square curve fitting analysis of XPS N1s spectra. The pyridinic N and graphitic N component peaks were assigned at 398.5 and 401.1 eV, respectively. The active sites of the N-doped HOPG surface were then subjected to oxygen reduction reaction and followed by XPS characterization. It was found that

the concentration of pyridinic N decreased, while the concentration of pyridonic N increased. This result suggests that the C atom next to pyridinic N is the active site, which reacts with the OH species formed during the oxygen reduction reaction, accompanied by the transformation of the pyridinic N to the pyridonic N.

Surface functionalization of graphene and graphite is also an essential process to enable them to be used for various applications owing to the changes of the surface chemistry such as hydrophobicity and hydrophilicity. For example, hydrogenation reaction is a common way to introduce C-H bonds on the surfaces of graphene and graphite by converting $sp^2$ carbons to $sp^3$ carbons [39]. Birch reduction has been used to convert localized $sp^2$ carbons to $sp^3$ carbons at the edges of the graphite surface without creating additional defects in the graphite structure [40, 41]. **Figure 7a** shows a comparison of C1s spectra of graphite powder and hydrogenated graphite powder and a curve-fitting analysis of the two spectra. From the XPS measurements of graphite and hydrogenated graphite powders annealed at 500°C, the binding energy of the C1s main peak of the hydrogenated graphite powder shifted by 0.4 eV toward the high-binding-energy compared to that of the graphite powder [42]. In the C1s spectrum of the graphite powder, only a dominant component peak representing $sp^2$ carbons and a small component peak representing $sp^3$ carbons are observed. The decrease and increase in the intensity of the $sp^2$ and $sp^3$ carbon component peaks, respectively, observed in the C1s spectrum of the hydrogenated graphite powder confirm the conversion of $sp^2$ to $sp^3$ carbons. However, one key disadvantage of using XPS in the above analysis is that XPS cannot detect H and exactly confirm the increase in the hydrogen concentration on a hydrogenated graphite powder surface. By contrast, ToF-SIMS is extremely sensitive to hydrogen and can be used for this purpose instead. Both the ToF-SIMS negative ion spectra of graphite and hydrogenated graphite powders show $C_x^-$ and $C_xH^-$ ion series; nevertheless, the major difference between these two spectra is the increase of normalized intensities of the $H^-$ and $C_xH^-$ ions after hydrogenation (**Figure 7b**), strongly indicating a higher concentration of hydrogen on the hydrogenated graphite powder surface.

Functionalization of graphene and graphite usually involves oxidation of their surfaces by different processes [43]. Graphene and graphite oxides are compounds consisting of carbon, oxygen and hydrogen with different ratios, obtained by
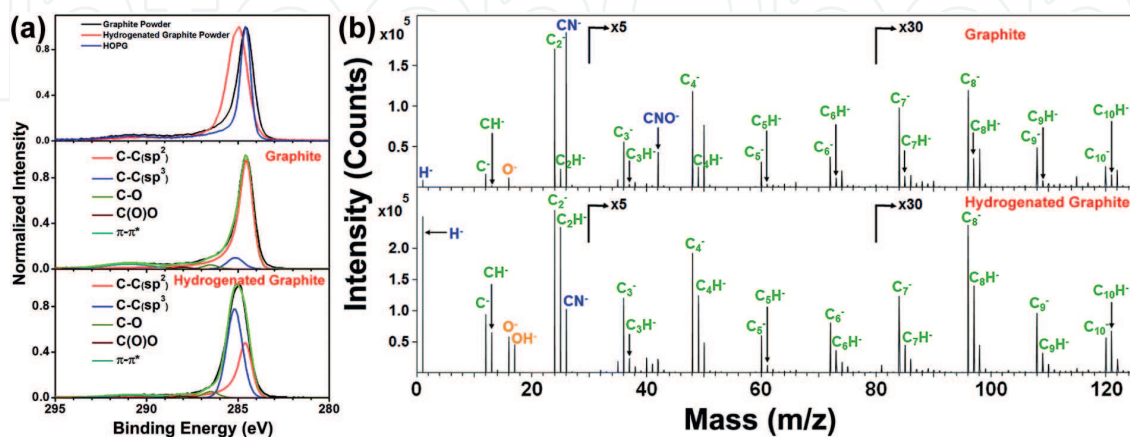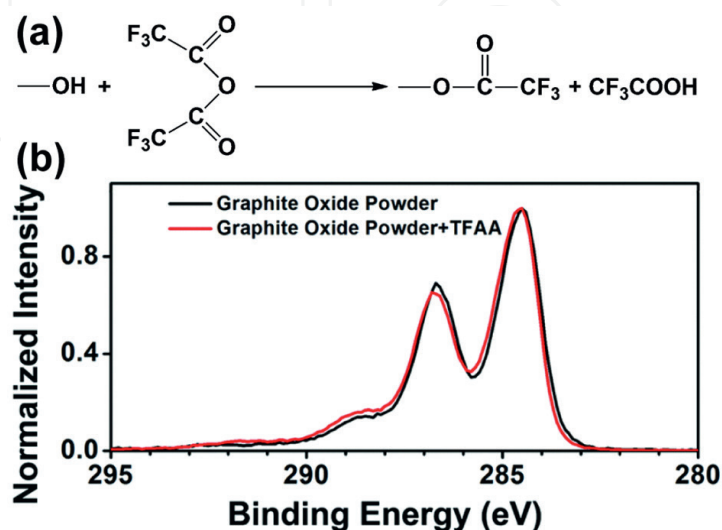


**Figure 7.**
*(a) A comparison of the XPS C1s spectra of the HOPG, graphite powder and hydrogenated graphite powder, XPS C1s curve-fitting results for graphite powder and hydrogenated graphite powder after annealing at 500°C. The black (—) and green (—) lines represent the experimental and curve-fitted spectra, respectively. (b) ToF-SIMS negative ion spectra of graphite powder and hydrogenated graphite powder after annealing at 500°C [42].*

treating graphite with strong oxidizers. One common method to produce graphene and graphite oxides is the modified Hummers' method (MHM) [44, 45]. The oxidation results in incorporation of hydroxyl and epoxy groups into the basal plane and carboxyl groups at the edges of graphene and graphite [46]. The existence of these functional groups, of which the chemical states and concentrations, can be determined by XPS. One of the key difficulties to differentiate between hydroxyl and epoxy groups is due to their similar C1s binding energies. To solve this problem, chemical derivatization XPS has been commonly used. Trifluoroacetic anhydride (TFAA) chemical derivatization has been applied to quantify the hydroxyl groups on different surfaces [47, 48]. TFAA mainly reacts with the hydroxyl groups, leading to the formation of $CF_3$ and ester carbons with identical concentrations on the surface (**Figure 8a**). After the TFAA derivatization, the peak, which originally corresponds to epoxy and hydroxyl groups, becomes mainly associated with the epoxy groups. Following this ideal, graphite oxide powder was first prepared using the MHM. The surface of this resulting graphite oxide powder was analyzed by XPS and the results show that the surface mainly consists of C (74.4 at%) and O (25.2 at%) [49]. After the labeling of the hydroxyl groups with TFAA, a small decrease of the C-O concentration is observed as shown in **Figure 8b**, and only 1.4 at% of F was detected. According to the reaction mechanism, the reaction between one TFAA molecule and one hydroxyl group introduces three F atoms on surface, this means that the carbons representing the hydroxyl groups should be less than 0.5 at% and the C-O component peak in the C1s spectrum of graphite oxide powder is mostly due to epoxy groups on the surface.

The oxygen-containing functional groups on the surfaces of graphene and graphite oxides can be further modified with different molecules through covalent or noncovalent bonds. Theoretical calculations have shown that the epoxy groups on graphene and graphite oxide surfaces play an important role in the reactions with different gases, such as oxidizing $SO_2$ to $SO_3$ at room temperature [50]. Based on the XPS result showing that graphite oxide powder prepared using the MHM contains epoxy groups, the reaction between the graphite oxide powder prepared by MHM and $SO_2$ was carried out [49]. The reaction between the graphite oxide powder and $SO_2$ produced about 3.8 at% of S on its surface. A comparison of the spectra (**Figure 9a** and **b**) of



**Figure 8.**
*(a) Reaction mechanism between TFAA and the hydroxyl group on a surface. (b) A comparison of C1s spectra of graphite oxide powder before and after the reaction with TFAA at 25°C [49].*
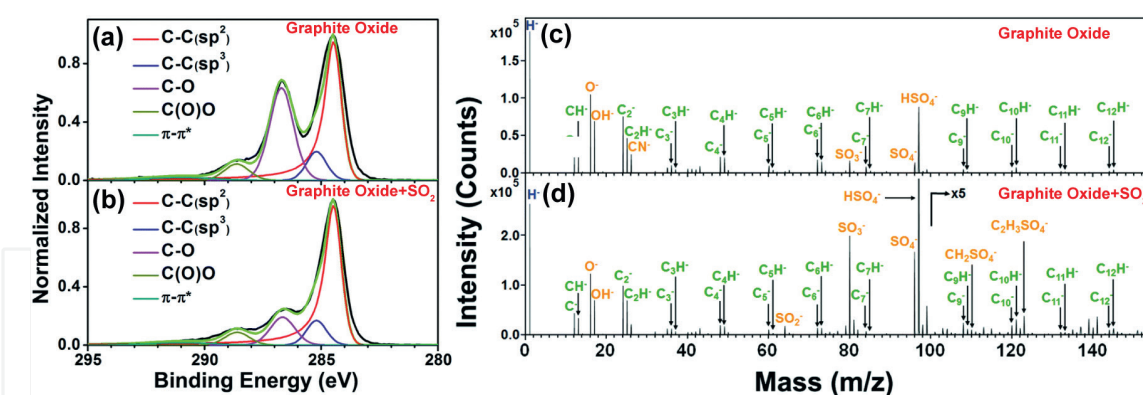
**Figure 9.**
*XPS C1s normalized spectra of graphite oxide powder (a) before and (b) after the reaction with SO₂ obtained at 25°C. The black (—) and green (—) lines represent the experimental and curve-fitted spectra, respectively. ToF-SIMS negative ion spectra of graphite oxide powder (c) before and (d) after the reaction with SO₂ obtained at 25°C [49].*

graphite oxide powder before and after the reaction shows that the C-O peak decreases while peak representing the carboxyl group almost stays the same after the reaction, suggesting that the $SO_2$ mainly reacts with the epoxy groups to produce the $C-O-SO_3H$ groups. ToF-SIMS spectra of graphite oxide powder before and after the reaction with $SO_2$ were acquired. The $C_x^-$ and $C_xH^-$ ion series representing the graphite peaks are the dominant components in the ToF-SIMS negative ion spectrum of graphite oxide powder (**Figure 9c**). After the reaction between the graphite oxide powder and $SO_2$, the sulfate-related peaks, such as $HSO_4^-$ and $SO_4^-$, become the dominant peaks in the spectrum (**Figure 9d**). The changes can also be seen from the increase of normalized ion intensities of $HSO_4^-$, $SO_4^-$ and $SO_3^-$ ions after the reaction with $SO_2$. In addition, the intensities of $CH_2SO_4^-$ and $C_2H_3SO_4^-$ ions also increase, indicating that most of the $SO_2$ had reacted at and attached to the oxidation sites on the surface of the graphite oxide powder. In summary, the epoxy groups on the surface of the graphite oxide powder are responsible for the oxidation of $SO_2$ into bisulfate.

## 6. Conclusions

Graphene and graphite have been widely used in various applications owing to their special properties and structures. In particular, the surface properties of graphene and graphite are vital to the performance of many products utilizing these materials. XPS and ToF-SIMS are two main surface analysis techniques that have been used extensively and successfully to study the composition, structure, cleanliness, defects, and reactions of graphene and graphite surfaces. XPS is widely used to yield quantitative elemental and chemical state information of graphene and graphite surfaces. ToF-SIMS provides chemical composition and detailed molecular structure information of graphene and graphite surfaces with high sensitivity. A combination of XPS and ToF-SIMS has been shown to provide complementary information allowing a full and in-depth understanding of graphene and graphite surfaces, which facilitates the transition from fundamental research to practical applications.

## Author details

Wenjing Xie[1]* and Chi-Ming Chan[2,3]

1 College of Chemistry, Beijing Normal University, Beijing, China

2 Division of Environment and Sustainability, Hong Kong University of Science and Technology, Kowloon, Hong Kong

3 Department of Chemical and Biological Engineering, Hong Kong University of Science and Technology, Kowloon, Hong Kong

*Address all correspondence to: wjxie@bnu.edu.cn

IntechOpen

## References

[1] Geim AK, Novoselov KS. The rise of graphene. Nature Materials. 2007;**6**:183-191

[2] Schwierz F. Graphene transistors. Nature Nanotechnology. 2010;**5**:487-496

[3] Lin Y-M, Valdes-Garcia A, Han S-J, Farmer DB, Meric I, Sun Y, et al. Wafer-scale graphene integrated circuit. Science. 2011;**332**:1294-1297

[4] Nair RR, Blake P, Grigorenko AN, Novoselov KS, Booth TJ, Stauber T, et al. Fine structure constant defines visual transparency of graphene. Science. 2008;**320**:1308-1308

[5] Balandin AA, Ghosh S, Bao W, Calizo I, Teweldebrhan D, Miao F, et al. Superior thermal conductivity of single-layer graphene. Nano Letters. 2008;**8**:902-907

[6] Wang Y, Chen X, Zhong Y, Zhu F, Loh KP. Large area, continuous, few-layered graphene as anodes in organic photovoltaic devices. Applied Physics Letters. 2009;**95**:063302

[7] Liu J, Bao S, Wang X. Applications of graphene-based materials in sensors: A review. Micromachines. 2022;**13**:184

[8] Seo G, Lee G, Kim MJ, Baek S-H, Choi M, Ku KB, et al. Rapid detection of COVID-19 causative virus (SARS-CoV-2) in human nasopharyngeal swab specimens using field-effect transistor-based biosensor. ACS Nano. 2020;**14**:5135-5142

[9] Chang H, Bard AJ. Observation and characterization by scanning tunneling microscopy of structures generated by cleaving highly oriented pyrolytic graphite. Langmuir. 1991;**7**:1143-1153

[10] Mándi G, Teobaldi G, Palotás K. Contrast stability and 'stripe' formation in scanning tunnelling microscopy imaging of highly oriented pyrolytic graphite: The role of STM-tip orientations. Journal of Physics. 2014;**26**:485007

[11] Yang S, Tsai P, Kooij ES, Prosperetti A, Zandvliet HJW, Lohse D. Electrolytically generated nanobubbles on highly oriented pyrolytic graphite surfaces. Langmuir. 2009;**25**:1466-1474

[12] Lu X, Huang H, Nemchuk N, Ruoff RS. Patterning of highly oriented pyrolytic graphite by oxygen plasma etching. Applied Physics Letters. 1999;**75**:193-195

[13] Chan C-M, Weng L-T. Applications of X-ray photoelectron spectroscopy and static secondary ion mass spectrometry in surface characterization of copolymers and polymers blends. Reviews in Chemical Engineering. 2000;**16**:341-408

[14] Chan C-M, Weng L-T. Surface characterization of polymer blends by XPS and ToF-SIMS. Materials. 2016;**9**:655

[15] Abidi IH, Weng L-T, Wong CPJ, Tyagi A, Gan L, Ding Y, et al. New approach to unveiling individual atomic layers of 2D materials and their heterostructures. Chemistry of Materials. 2018;**30**:1718-1728

[16] Mattevi C, Kim H, Chhowalla M. A review of chemical vapour deposition of graphene on copper. Journal of Materials Chemistry. 2011;**21**:3324-3334

[17] Li X, Cai W, An J, Kim S, Nah J, Yang D, et al. Large-area synthesis of high-quality and uniform graphene films on copper foils. Science. 2009;**324**:1312-1314

[18] Khomyakov PA, Giovannetti G, Rusu PC, Brocks G, van den Brink J, Kelly PJ. First-principles study of the interaction and charge transfer between graphene and metals. Physical Review B. 2009;**79**:195425

[19] Xie W, Haider Abidi I, Luo Z, Weng L-T, Chan C-M. Characterization of the interaction between graphene and copper substrate by time-of-flight secondary ion mass spectrometry. Applied Surface Science. 2021;**544**:148950

[20] Suk JW, Kitt A, Magnuson CW, Hao Y, Ahmed S, An J, et al. Transfer of CVD-grown monolayer graphene onto arbitrary substrates. ACS Nano. 2011;**5**:6916-6924

[21] Li X, Zhu Y, Cai W, Borysiak M, Han B, Chen D, et al. Transfer of large-area graphene films for high-performance transparent conductive electrodes. Nano Letters. 2009;**9**:4359-4363

[22] Pirkle A, Chan J, Venugopal A, Hinojos D, Magnuson CW, McDonnell S, et al. The effect of chemical residues on the physical and electrical properties of chemical vapor deposited graphene transferred to $SiO_2$. Applied Physics Letters. 2011;**99**:122108

[23] Lin Y-C, Jin C, Lee J-C, Jen S-F, Suenaga K, Chiu P-W. Clean transfer of graphene for isolation and suspension. ACS Nano. 2011;**5**:2362-2368

[24] Xie W, Weng L-T, Ng KM, Chan CK, Chan C-M. Clean graphene surface through high temperature annealing. Carbon. 2015;**94**:740-748

[25] Wang X, Dolocan A, Chou H, Tao L, Dick A, Akinwande D, et al. Direct observation of poly(methyl methacrylate) removal from a graphene surface. Chemistry of Materials. 2017;**29**:2033-2039

[26] Lupina G, Kitzmann J, Costina I, Lukosius M, Wenger C, Wolff A, et al. Residual metallic contamination of transferred chemical vapor deposited graphene. ACS Nano. 2015;**9**:4776-4785

[27] Batzill M. The surface science of graphene: Metal interfaces, CVD synthesis, nanoribbons, chemical modifications, and defects. Surface Science Reports. 2012;**67**:83-115

[28] Xie W, Weng L-T, Ng KM, Chan CK, Chan C-M. Defects of clean graphene and sputtered graphite surfaces characterized by time-of-flight secondary ion mass spectrometry and X-ray photoelectron spectroscopy. Carbon. 2017;**112**:192-200

[29] Doniach S, Sunjic M. Many-electron singularity in X-ray photoemission and X-ray line spectra from metals. Journal of Physics C: Solid State Physics. 1970;**3**:285-291

[30] Yang DQ, Sacher E. s-p hybridization in highly oriented pyrolytic graphite and its change on surface modification, as studied by X-ray photoelectron and Raman spectroscopies. Surface Science. 2002;**504**:125-137

[31] Kholmanov IN, Edgeworth J, Cavaliere E, Gavioli L, Magnuson C, Ruoff RS. Healing of structural defects in the topmost layer of graphite by chemical vapor deposition. Advanced Materials. 2011;**23**:1675-1678

[32] Zion E, Butenko A, Kaganovskii Y, Richter V, Wolfson L, Sharoni A, et al. Effect of annealing on Raman spectra of monolayer graphene samples gradually disordered by ion irradiation. Journal of Applied Physics. 2017;**121**:114301

[33] Huang Q, Li J, Liu R, Yan L, Huang H. Surface morphology and microstructure evolution of IG-110

graphite after xenon ion irradiation and subsequent annealing. Journal of Nuclear Materials. 2017;**491**:213-220

[34] Xie W, Weng L-T, Yeung KL, Chan C-M. Repair of defects created by Ar$^+$ sputtering on graphite surface by annealing as confirmed using ToF-SIMS and XPS. Surface and Interface Analysis. 2018;**50**:851-859

[35] Lesiak B, Zemek J, Houdkova J, Kromka A, Oacute ZA. Electron spectra line shape analysis of highly oriented pyrolytic graphite and nanocrystalline diamond. Analytical Sciences. 2010;**26**:217-222

[36] Mezzi A, Kaciulis S. Surface investigation of carbon films: From diamond to graphite. Surface and Interface Analysis. 2010;**42**:1082-1084

[37] Dai L, Xue Y, Qu L, Choi H-J, Baek J-B. Metal-free catalysts for oxygen reduction reaction. Chemical Reviews. 2015;**115**:4823-4892

[38] Guo D, Shibuya R, Akiba C, Saji S, Kondo T, Nakamura J. Active sites of nitrogen-doped carbon materials for oxygen reduction reaction clarified using model catalysts. Science. 2016;**351**:361-365

[39] Nikitin A, Näslund L-Å, Zhang Z, Nilsson A. C-H bond formation at the graphite surface studied with core level spectroscopy. Surface Science. 2008;**602**:2575-2580

[40] Yang Z, Sun Y, Alemany LB, Narayanan TN, Billups WE. Birch reduction of graphite. Edge and interior functionalization by hydrogen. Journal of the American Chemical Society. 2012;**134**:18689-18694

[41] Pekker S, Salvetat JP, Jakab E, Bonard JM, Forró L. Hydrogenation of carbon nanotubes and graphite in liquid ammonia. The Journal of Physical Chemistry B. 2001;**105**:7938-7943

[42] Xie W, Ng KM, Weng L-T, Chan C-M. Characterization of hydrogenated graphite powder by X-ray photoelectron spectroscopy and time-of-flight secondary ion mass spectrometry. RSC Advances. 2016;**6**:80649-80654

[43] Zhu Y, Murali S, Cai W, Li X, Suk JW, Potts JR, et al. Graphene and graphene oxide: Synthesis, properties, and applications. Advanced Materials. 2010;**22**:3906-3924

[44] Dimiev AM, Tour JM. Mechanism of graphene oxide formation. ACS Nano. 2014;**8**:3060-3068

[45] Poh HL, Šaněk F, Ambrosi A, Zhao G, Sofer Z, Pumera M. Graphenes prepared by Staudenmaier, Hofmann and Hummers methods with consequent thermal exfoliation exhibit very different electrochemical properties. Nanoscale. 2012;**4**:3515-3522

[46] Dreyer DR, Park S, Bielawski CW, Ruoff RS. The chemistry of graphene oxide. Chemical Society Reviews. 2010;**39**:228-240

[47] Rinsch CL, Chen X, Panchalingam V, Eberhart RC, Wang J-H, Timmons RB. Pulsed radio frequency plasma polymerization of allyl alcohol: Controlled deposition of surface hydroxyl groups. Langmuir. 1996;**12**:2995-3002

[48] Chilkoti A, Ratner BD, Briggs D. Plasma-deposited polymeric films prepared from carbonyl-containing volatile precursors: XPS chemical derivatization and static SIMS surface characterization. Chemistry of Materials. 1991;**3**:51-61

[49] Xie W, Weng L-T, Chan C-K, Yeung KL, Chan C-M. Reactions of $SO_2$ and $NH_3$ with epoxy groups on the surface of graphite oxide powder. Physical Chemistry Chemical Physics. 2018;**20**:6431-6439

[50] Cen W, Hou M, Liu J, Yuan S, Liu Y, Chu Y. Oxidation of $SO_2$ and NO by epoxy groups on graphene oxides: The role of the hydroxyl group. RSC Advances. 2015;**5**:22802-22810